Results in Engineering 16 (2022) 100735

Contents lists available at ScienceDirect

Results in Engineering

journal homepage: www.sciencedirect.com/journal/results-in-engineering

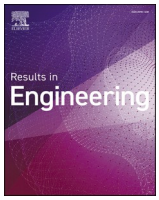

A novel CO2 thermal management system with battery two-phase (evaporative) cooling for electric vehicles

Xiang Yin [a], Jianmin Fang [a], Anci Wang [a], Yulong Song [a], Feng Cao [a,*], Xiaolin Wang [b]

[a] School of Energy and Power Engineering, Xi'an Jiaotong University, 28 Xianning West Road, Xi'an, 710049, China
[b] School of Engineering, University of Tasmania, Private bag 65, Hobart, TAS 7001, Australia

ARTICLE INFO

Keywords:
CO2 thermal management system
Battery two-phase cooling
Vapor quality
Evaporative cooling
Automobile air conditioner

ABSTRACT

Development of electric vehicles promotes an increasing demand for battery cooling, and secondary loop with glycol aqueous is widely used. However, the cooling performance is restricted, and it is heavily affected by the thermal delay because of large heat capacities. Two-phase evaporative cooling was demonstrated to have a better performance, but was disturbed by the potential thermal runway propagation of battery, due to the instability of evaporative cooling in chiller. In the presented paper, an effective solution was proposed based on a novel evaporative cooling system with transcritical CO2 cycles, which could always avoid this problem by a simple control strategy. Moreover, a control logical was set up and it was easy to achieve the energy management for cabin and battery. A mathematical model was developed, and it was validated by experiment. The vapor quality, cooling performance and flow velocity distributions were investigated at different operation conditions. Results showed that it could better deal with the problem of potential overheating and difficult-control. Under the condition of 0.5 kW battery power, the flow vapor quality along the channel increased from 0.23 to 0.94 of the conventional systems, while it only ranged from 0.23 to 0.4 in the proposed system. Additionally, the presented systems had 13.5%higher COP at the ambient temperature of 35 °C. It could be used in electric vehicles thermal management systems for efficient battery cooling.

1. Introduction

As the clean energy terminal, new energy automobiles, such as electric vehicles (EVs) [1], hybrid vehicles [2] and Hydrogen fuel cell vehicle have been attracted an increasing attention worldwide, to reduce the carbon footprint generated by conventional fuel-based vehicles of transportation. More efforts have been done for the development of the technologies, including the optimization of the core components [3] and the control strategy with intelligent technologies [4]. For EVs, an important component is a battery, and as of now, thermal safety issues of batteries is still the most unendurable discomfort point and the focus of research for technological enhancements [5]. Thus, thermal management for battery acts a significant role in the applications of EVs. Current approaches for battery cooling mostly contain forced convection cooling [6], secondary liquid-cooling [7], two-phase cooling [8], phase change material cooling [9], application of heat pipe [10], the combined cooling method with solid-state thermoelectric refrigeration [11] and so on.

Among all the cooling method for battery, air cooling such as natural or forced-air cooling was a simple and low cost thermal management system [12], but had limited heat dissipation capacity due to the relatively low thermal conductivity and heat transfer coefficient [13]. It was often used in the application that the battery had relatively low heat flux density. The dynamic cooling performance during charge process were optimized by different control strategies [14]. For the liquid cooling, including the heat pipe or fluid liquid cooling, was required to equip a complex system and an increasing cost. The cooling efficiency was enhanced in compared to the air cooling [5], and it could be also improved with the optimization of mass flow, clod plate number, cooling direction and other parameters [15]. Compared with air cooling, liquid cooling and PCM cooling, Karimi et al. [16] declared that the liquid cooling had the best performance, via the experiment and numerical analysis. Two-phase cooling was one of the liquid cooling but had a better performance thanks to the boiling flow, which had the higher heat transfer coefficient. Due to the increasing heat flux density, the secondary liquid-cooling and two-phase cooling had potential utilization for battery cooling, and phase change material and heat pipe were often used as the auxiliary method due to the restriction of cooling capacity. Research revealed that liquid metals, nanofluids, and boiling

* Corresponding author.
E-mail address: fcao@mail.xjtu.edu.cn (F. Cao).

https://doi.org/10.1016/j.rineng.2022.100735
Received 16 August 2022; Received in revised form 27 October 2022; Accepted 27 October 2022
Available online 1 November 2022

Nomenclature

Variable names

A	Heat transfer area, m^2
D	Diameter or characteristic length, mm
F_d	Fin depth, mm
F_l	Fin length, mm
F_p	Fin spacing, mm
F_t	Fin thickness, mm
G	Mass velocity, $kg{\cdot}m^{-2}{\cdot}s^{-1}$
f	Friction factor
H	Enthalpy, $kJ{\cdot}kg^{-1}$
h	Heat transfer coefficient $W{\cdot}m^{-2}{\cdot}K^{-1}$
L_p	Louver spacing, mm
m	Mass flow rate, $kg{\cdot}s^{-1}$
N_{LB}	Louver row number
Nu	Nusselt number
n	Compressor speed, $r{\cdot}min^{-1}$
P	Pressure, MPa
Pr	Prandtl number
T	Temperature, °C
T_P	Tube pitch, mm
Re	Reynolds number
Re_D	Reynolds number based on characteristic length
Re_{mod}	The modified Reynolds number
v	Velocity, $m{\cdot}s^{-1}$
V_d	Compressor displacement, cm^3
W	Power consumption, kW

GREEK SYMBOLS

ρ	Density, kg·m-3
η	Efficiency
θ	Fin angle, °
λ	Thermal conductivity, W·m-1·K-1
μ	kinematic viscosity, m2·s-1
σ	Surface tension, N·m-1
χ	Vapor quality

SUBSCRIPTS

dis	Discharge process
e	Electric efficiency
g	Gas state
is	Isentropic process
j	Kolben factor
l	Liquid state
suc	Suction
w	Wall material
v	Volumetric efficiency

liquids (two-phase cooling/evaporative cooling) were considered as the most prominent battery cooling methods owing to the higher thermal conductivity [13].

As for the two-phase refrigerant cooling system, taking advantage of the higher latent heat, constant medium temperature (saturation temperature), usually showed a larger amount of cooling capacity, higher heat transfer rate and minor temperature difference [17], when it was used for the battery cooling. Meanwhile, the pressure drop also strongly affected the comprehensive cooling results [18]. Two-phase evaporative cooling had a good performance, and the temperature distributions of the battery could be more homogeneous [19]. In addition, it had relatively uniform voltage distribution of battery modules at the operation of different discharge rates [20]. Maan Al-Zareer et al. [21]designed a boiling cooling system for hybrid electric vehicles using liquid propane, and results showed that the temperature was efficiently managed even at 7.5 charge-discharge rate. Moreover, Maan Al-Zareer et al. [22]. Further applied a tank using refrigerant R134a for the battery boiling cooling in electric vehicles, and it could limit the battery temperature rise to 1.6 °C. However, the system only worked when the air and cabin temperature was lower than 30 °C, and a further effective condensing devices might be required.

Inside the channel of the heat sink for battery two-phase cooling, the flow pattern was often determined by the vapor quality, and then the cooling performance was heavily influenced [23]. The same results were also drawn in the works of van Gils et al. [19] Huang et al. [24] conducted an experiment to investigate the performance of mini-channel heat sink for battery thermal management, and the influence of the refrigerant charge, throttling valve degree, heating power on the cooling performance were examined and analyzed. Wang et al. [25], conducted an experiment and mathematical model to reveal the performance of the boiling cooled battery thermal management system for electric vehicles, and results demonstrated that the battery temperature difference increased by the increase of the vapor fraction. In the study of da Silva Lima et al. [26], the heat transfer coefficient decreased sharply when the outlet vapor quality of the heat sink exceeded a certain value. Fang et al. [27] declared that overall heat transfer coefficient was heavily affected by the cold plate outlet vapor quality for the battery two-phase cooing, and the optimum outlet vapor quality was around 0.25 at the operation condition in the study. The similar conclusion from the previous work was that the vapor quality at the inlet and outlet of the heat sink act significantly on battery two-phase cooling performance.

Besides the thermal management for battery, the temperature control of the cabin is another important topic, which directly affect the cabin comfortable. In view of the composite demand, the integrated thermal management system both for cabin comfortable and battery thermal safety attracts more attentions. For the conventional integrated thermal management systems in electric vehicles, the chiller was usually in parallel with the evaporator that was used for cabin comfort, such as the works of Ma et al. [28] and Tian et al. [29] and so on. When it used in two-phase battery cooling, the vapor fraction at the outlet of the heat sink should be controlled to a proper value to avoid thermal runaway propagation, but the vapor fraction was hard to be commanded due to the difficulty of measurement, feedback regulation and the flow distributions. It was in dire need of more efficient technology to promote the application of two-phase battery cooling that was integrated with HVAC & HP (Heating Ventilation Air Conditioning and Heat Pump) system.

Additionally, in consideration of refrigerant substitution and heating problem of electric vehicles, transcritical CO2 cycles turns to be one of the most promising technology. However, the research was now only focused on the heating performance in winter [30] and the cooling performance in summer [31], and cooling performance of the cabin, or it was involved with the system optimization including the ejector [32], the gas cooler configuration [33], the intermediate cooling at the compressor process [34], the refrigerant charge [35], the internal heat transfer coefficient [36] and so on. There was few study on the thermal management of battery, especially two-phase battery cooling based on CO2 systems.

The previous works concluded that the two-phase battery cooling method had a better performance than that of the air cooling or secondary liquid cooling. However, the battery cooling performance was strongly affected by the vapor quality of the two-phase fluid, and the optimum vapor quality was usually not a larger value. Caused by nonuniformity of the two-phase flow distributions, this decreasing cooling performance would be deteriorated, leading to the battery thermal runaway propagation. Research demonstrated this conclusion but gave no effective solutions. The novelty of the paper was to deal with

the potential battery thermal runaway propagation of two-phase evaporative cooling.

In the presented study, it gave an effective solution to ensure the two-phase state and a lower vapor quality variation along the channel of battery chiller, thus the battery thermal runaway propagation was reduced even under the conditions of the nonuniformity flow distributions. A novel thermal management system within the two-phase cooling system was proposed to deal with the uncontrollable vapor quality problem, and an efficient control logic was set up to ensure the two-phase state of the heat sink outlet. This provided an effective solution for the two-phase refrigerant cooling applied in the practical engineering.

2. Different thermal management system

For the two-phase refrigerant battery cooling, it was often required a compression refrigeration system to provide a temperature adjustable working medium. In the electric vehicle, an increasing demand of integrated thermal management system was developed for a more efficient energy utilization, equipped with the cabin temperature control, battery, and electronic components temperature management. For the cooling demand, the battery heat exchanger in parallel with the cabin evaporator was widely used in the conventional thermal management system, as depicted in Fig. 1. Two expansion valves were placed in each branch, respectively, to provide the required cooling capacity. In a transcritical CO2 cycle, an internal heat exchanger was applied for a better system performance. There were two series heat exchangers in the Heating Ventilation Air Conditioning Cabinet (HVAC) for the cabin cooling. This system could supply cold water for the battery cooling when it was used for liquid cooling (water cooling), and the water-cooling performance was less affected by the variable heat transfer coefficient along the flow channel of the battery heat exchanger. However, for the two-phase refrigerant cooling, this variable heat transfer coefficient would result in the non-homogenous battery temperature, caused by the variable vapor quality or even superheated refrigerant.

To deal with this problem, a novel thermal management system for two-phase battery cooling was proposed, as shown in Fig. 1b. In this system configuration, the battery cold plate was placed before one of the air heat exchangers in HVAC, which could benefit the heat transfer performance of the flow at the outlet of cold plate.

For the two systems, the compressor displacement was both 6.8 mm^3, and the maximum rotational speed was 8600 r•min-1. The outside and inside heat exchanger were both fin-tube heat exchangers with the micro-channel. For the outside heat exchanger, which was used for heat exchanging with ambient air, was a single-row component. The length and the width were 600 mm and 300 mm, respectively. The thickness was 20 mm. With respect to the inside heat exchanger, the inside heat exchanger 1 had the size of 218 mm × 200 mm × 38 mm, and the exchanger 2 had the size of 156 mm × 142 mm × 32 mm. The volume of the accumulator was 500 ml.

In the presented study, the operation condition and the key parameters of the two-systems was depicted in Table 1.

3. Mathematical model of the system

The mathematical model was established with the assistant of the commercial software GT-suite. The system model was combined with the different component models. The simulation results were considered as the stable value when the fluctuation of the parameters was lower than 0.01%.

3.1. Model of compressor

The compressor follows the model of volumetric efficiency, isentropic efficiency, electrical efficiency. The mass flow rate of the compressor is calculated as follows.

$$\dot{m} = \frac{1}{60}\rho_{suc} \bullet \eta_v \bullet n \bullet V_d \quad 3\text{-}1$$

where ρ_{suc} is the suction density, and η_v is the volumetric efficiency. n and V_d are the compressor speed and displacement, respectively.

The compressor work is calculated according to the following equation.

$$W = \frac{\dot{m}(H_{dis-is} - H_{suc})}{\eta_e \bullet \eta_{is}} \quad 3\text{-}2$$

where η_e and η_{is} are the electrical efficiency and isentropic efficiency of the compressor. H_{dis-is} and H_{suc} are the discharge and suction enthalpy of the compressor, respectively.

The volumetric efficiency, isentropic efficiency and electrical efficiency are obtained as below.

$$\eta_v = 1.1531 \bullet r^{-0.308} \quad 3\text{-}3$$

$$\eta_{is} = 0.9127 \bullet r^{-0.3563} \quad 3\text{-}4$$

$$\eta_e = 0.8931 \bullet r^{0.0133} \quad 3\text{-}5$$

3.2. The heat transfer model

For the CO2 side, the heat transfer correlation of Sieder-Tate is used for the heat transfer of supercritical state.

$$Nu = 0.027 \cdot Re_D^{0.8} \cdot Pr^{\frac{1}{3}} \frac{\mu}{\mu_{sm}} \quad 3\text{-}6$$

where μ and μ_s are the dynamic viscosity and kinematic viscosity, respectively.

The heat transfer coefficient of CO_2 side is calculated as follows.

$$h = \mathrm{Nu}\frac{\lambda}{D} \quad 3\text{-}7$$

where λ and D thermal conductivity and characteristic length of the flow channel.

For the evaporation process in the evaporator, the heat transfer coefficient follows the below equations.

$$h = 0.087 Re_{mod}^{0.6} Pr_l^{1/6} \left(\frac{\rho_g}{\rho_l}\right)^{0.2} \left(\frac{\lambda_w}{\lambda_l}\right)^{0.09} \frac{\lambda_l}{b} \quad 3\text{-}8$$

$$\mathrm{Re_{mod}} = \frac{w_m b}{v_l} \quad 3\text{-}9$$

$$w_m = \frac{\rho v}{\rho_l}\left(1 + x\left(\frac{\rho_l}{\rho_g} - 1\right)\right) \quad 3\text{-}10$$

$$b = \sqrt{\frac{\sigma}{g(\rho_l - \rho_g)}} \quad 3\text{-}11$$

where $\mathrm{Re_{mod}}$ is the modified Reynolds number.

For the single phase heat transfer, the D-B correlation [37] is used.

$$\mathrm{Cooling} \rightarrow \mathrm{h} = 0.023 \cdot \mathrm{Re}^{0.8} \cdot \mathrm{Pr}^{0.3} \frac{\lambda}{\mathrm{D}} \quad 3\text{-}12$$

$$\mathrm{Heating} \rightarrow \mathrm{h} = 0.023 \cdot \mathrm{Re}^{0.8} \cdot \mathrm{Pr}^{0.4} \frac{\lambda}{\mathrm{D}} \quad 3\text{-}13$$

For the air side, the heat exchanger fin is corrugated fin with shutters, and the heat transfer coefficient is calculated according to Flat, Louver, Park-Jacobi.

$$h_a = Nu_a \frac{\lambda_a}{D_a} \quad 3\text{-}14$$

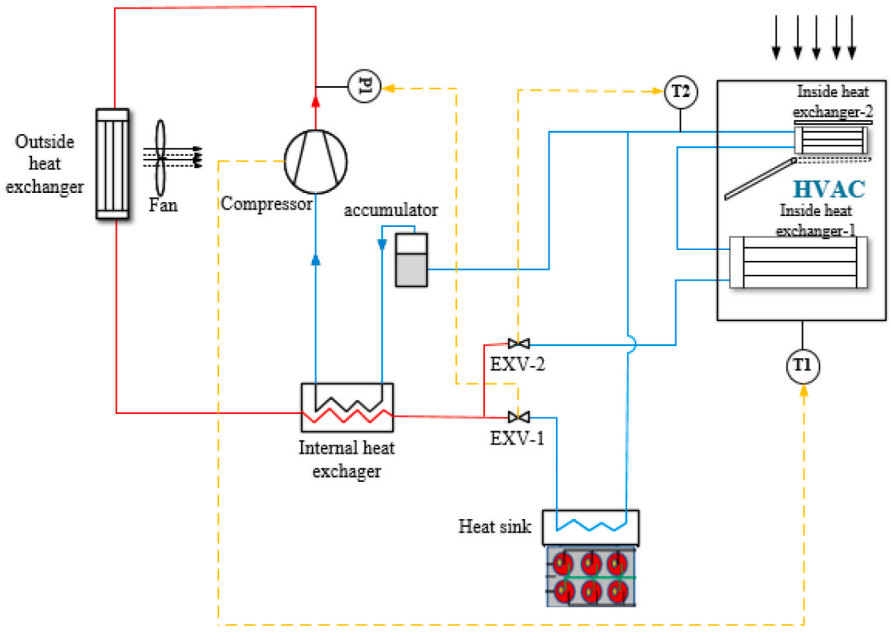

(a) The conventional thermal management system for two-phase battery cooling (system 1: Parallel configuration for battery cooling)

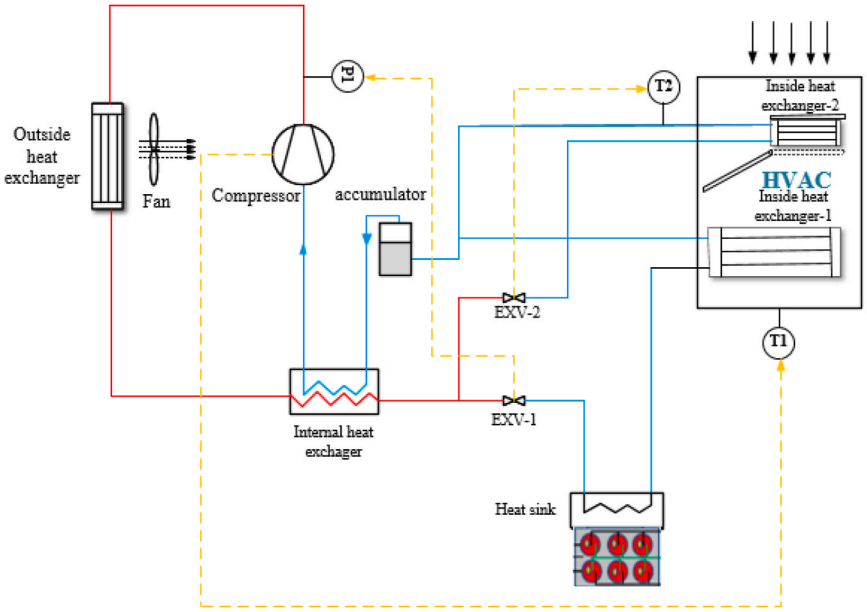

(b) The novel thermal management system for two-phase battery cooling (system 2: Series configuration for battery cooling)

Fig. 1. Thermal management systems for two-phase battery cooling with different configuration of battery cooling

At the steady operation condition, the compressor frequency and the opening degree of the expansion values were adjusted to meet the cooling requirements of the cabin and the battery. Moreover, the transcritical CO_2 system was usually required to be operated at an optimum discharge pressure for the best energy efficiency. For these objectives, the PID controller was used in the presented study. The compressor frequency was controlled for the requirement of supply air temperature, and the discharge pressure was obtained via the opening degree of EXV1. In order to avoid the superheated degree at the outlet of battery cold plate, the opening degree of EXV2 was adjusted to guarantee superheated temperature at the flow branch without battery cooling. The control logic was also depicted in Fig.1.

Table 1
The operation conditions and the key parameters.

Parameters	Values or value ranges
Ambient temperature	35 °C
HVAC inlet temperature and humidity	27 °C/50%
Heat load of the battery	0.2 kW、0.5 kW
Air flow rate of HVAC	450 m^3/h
Discharge pressure	Optimizing
Vapor quality of the heat exchanger for cabin	1 °C–5 °C

$$j=\frac{Nu_a}{Re_a\cdot Pr_a^{1/3}} \tag{3-15}$$

$$j=0.872 j_{Re} j_{low} j_{louver}\left(\frac{\theta\pi}{180}\right)^{0.219} N_{LB}^{-0.0881}\left(\frac{F_l}{L_P}\right)^{0.149}\left(\frac{F_d}{F_P}\right)^{-0.259}\left(\frac{L_l}{F_l}\right)^{0.54} * \left(\frac{F_l}{T_P}\right)^{-0.902}\left(1-\frac{F_t}{L_P}\right)^{2.62}\left(\frac{L_p}{F_p}\right)^{0.301} \tag{3-16}$$

$$j_{Re}=Re_{Lp}^{\left[-0.458+0.00874*\cosh\left(\frac{F_p}{L_p}-1\right)\right]} \tag{3-17}$$

$$j_{low}=1-\sin\left(\frac{L_p}{F_p}\bullet\theta\right)\left[\cosh\left(0.049Re_{Lp}-0.142\frac{F_d}{N_{LB}F_P}\right)\right]^{-1} \tag{3-18}$$

$$j_{louver}=1+0.0065\tan(\theta)\frac{F_d}{N_{LB}F_P}\cos\left[2\pi\left(\frac{F_p}{L_p\tan(\theta)}\right)-1.8\right] \tag{3-19}$$

where N_{LB} and F_l are louver row and fin length. L_P and F_d are louver spacing and fin depth. L_l and T_P are louver length and tube pitch. F_t and θ fin thickness and angle.

The heat transfer model is adapted to the gas cooler, the evaporator and the pipe, according to the flow state.

3.3. Pressure drop model

For the supercritical CO2 flow, the friction is calculated by the pipe flow model.

$$f=\begin{cases}\dfrac{16}{Re_D}, Re_D<Re_{cr}\\ \dfrac{0.08}{Re_D^{0.25}}, Re_D>4000\end{cases} \tag{3-20}$$

where Re_{cr} is critical Reynolds number.

When the Reynolds number is between the critical value and 4000, the friction is obtained by linear interpolation. For the smooth channel, the Re_D number is adjusted by the following equations.

$$Re_{D_{eff}}=Re_D\frac{16}{\left(C_f Re_D\right)_{lam}} \tag{3-21}$$

$$\left(C_f Re_D\right)_{lam}=24\left(1-1.3553\alpha+1.9467\alpha^2-1.7012\alpha^3+0.9564\alpha^4-0.2537\alpha^5\right) \tag{3-22}$$

For the two-phase side, the CO2 friction factor is calculated by the Friedel model, which is corrected form the Pipe Flow model by the correction factor Φ^2.

$$\Phi^2=E+\frac{3.24FH}{Fr_h^{0.045}We_l^{0.035}} \tag{3-23}$$

where

$$Fr_h=\frac{G^2}{gD\rho_h^2} \tag{3-24}$$

$$We_l=\frac{G^2D}{\sigma\rho_h^2} \tag{3-25}$$

$$\rho_{\langle}=\left(\frac{x}{\rho_g}+\frac{1-x}{\rho_l}\right)^{-1} \tag{3-26}$$

$$E=(1-x)^2+x^2\frac{\rho_l}{\rho_g}\frac{f_g}{f_l} \tag{3-27}$$

$$F=x^{0.78}(1-x)^{0.224} \tag{3-28}$$

$$H=\left(\frac{\rho_l}{\rho_g}\right)^{0.91}\left(\frac{\mu_g}{\mu_l}\right)^{0.19}\left(1-\frac{\mu_g}{\mu_l}\right)^{0.7} \tag{3-29}$$

where Fr_h is the froude number, and We_l is the weber number. G was the mass velocity. ρ_g and ρ_l are the density of vapor and liquid. μ_g and μ_l are the viscosity of vapor and liquid. ρ_h is the average density of the CO2 flow.

The pressure drop model is adapted to the gas cooler, the evaporator and the pipe, according to the flow state.

3.4. The gas-liquid separator model

A tank model is used for the gas-liquid separator model, and the liquid volume fraction (LVF) is calculated as below.

$$LVF=\frac{V_{liquid}}{V_{liquid}+V_{vapor}} \tag{3-30}$$

where LVF is the liquid volume fraction, V_{liquid} is the volume of liquid and V_{vapor} is the volume of vapor. LVF may varies from 0 (pure vapor) to 1 (pure liquid).

3.5. EXV model

The EXV is considered as an orifice valve model, and the rejection pressure is controlled by adjusting the flow area of the valve. For the orifice valve model, the multiplier to the friction loss coefficient is applied in the laminar region, and it is only used to the orifice faces with discontinuous area between the orifice and pipes. The friction loss coefficient K will be added to the momentum solution using the following relation based on Sisavath et al., 2002 [38]:

$$k=M_{LFF}M_{global,const}\frac{6\pi(M_1(1-AR_1)+M_2(1-AR_2))}{Re} \tag{3-31}$$

where: M_{LFF} is Laminar Face Friction Multiplier, $M_{global,const}$ is Global friction multiplier. AR_1 and AR_2 are the ratio of orifice area to upstream and downstream pipe area, respectively. M_1 and M_2 are Friction multiplier of upstream and downstream pipe or flow split part, respectively.

4. Result discussion

4.1. Experiment validation

To verify the reliability of the mathematical model in the presented paper, the cooling capacity and the compressor power under different operation condition were validated by the experimental data. For the working conditions, the ambient temperature varied from 25 to 45 °C, and the maximum air flow rate of HVAC was 480 m^3/h. Both internal cycle and fresh air cycle was tested in the experiment. The experimental facilities and measurement accuracy were referred to the work of Fang et al. [36] At the same operation conditions, the cooling capacity and compressor power of the experiment and simulations are depicted in Fig. 2. It could be obviously observed that the simulation error was

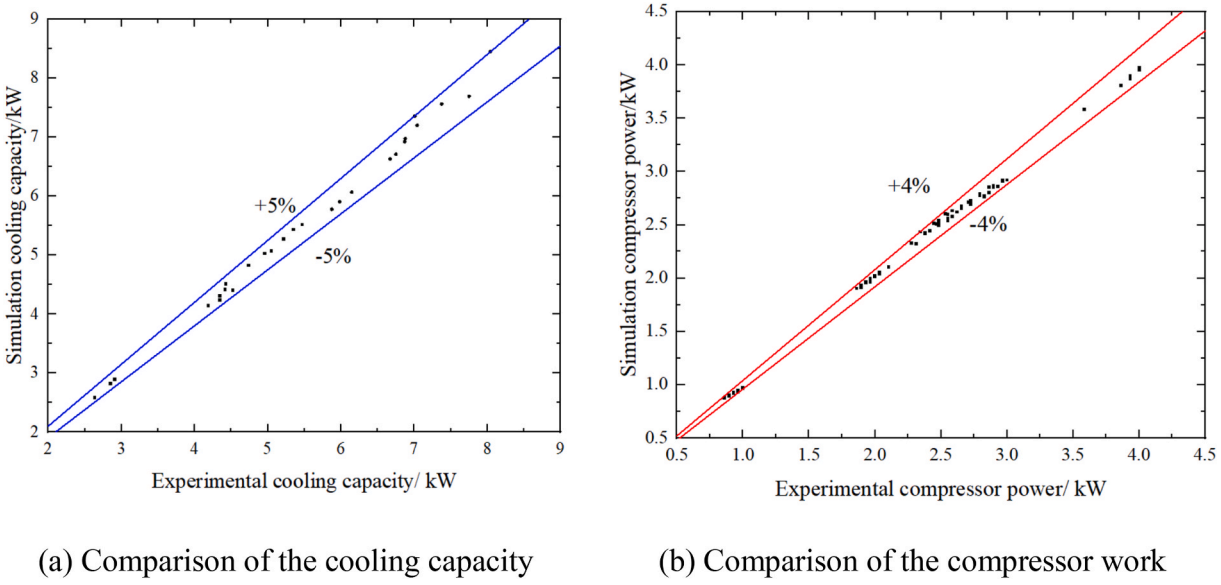

(a) Comparison of the cooling capacity (b) Comparison of the compressor work

Fig. 2. Validation of the simulation model.

about 5%, which represented that the simulation model in the presented study could be used for the result discussion and deep analysis of the thermodynamic characterize.

4.2. Vapor quality variation of the battery cooling channel

As the literal revealed, the vapor quality at the outlet of the battery cold-plate had a prominent influence on the actual cooling performance of the two-phase evaporative cooling. For the boiling heat transfer, the heat transfer coefficient was also strongly affected by the vapor quality and the flow-pattern of the two-phase flow. Thus, the smaller difference of vapor quality between inlet and outlet would benefit the temperature uniformity of the battery. For the larger difference of the vapor quality along the channel, this inhomogeneous flow would deteriorate the local vapor quality, even resulting in the local superheat and thermal runaway propagation. Fig. 3 gives the schematic diagram of the battery two-phase cooling, and the larger outlet vapor quality might directly cause the thermal runaway propagation at the local part of the battery.

Fig. 4 depicts the inlet and outlet vapor quality of the battery cold-plate under 0.5 kW power with the increasing superheat degree of air heat exchanger. Both system 1 and system 2 had the same operation condition. The ambient temperature was 35 °C, and the air inlet

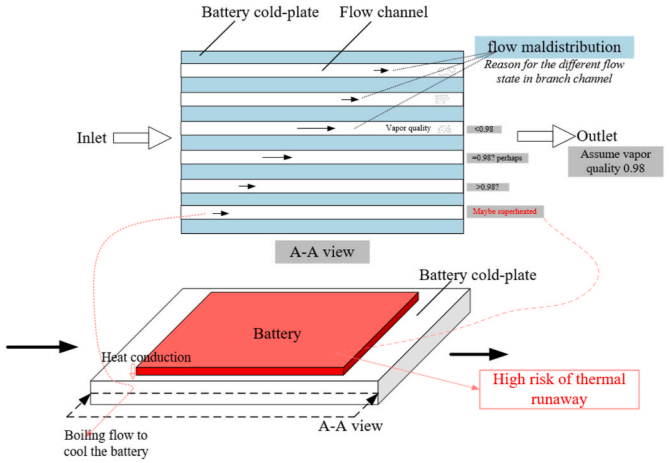

Fig. 3. Schematic diagram of the battery two-phase cooling.

temperature for the HVAC was 27 °C with 50% relative humidity. All the data was obtained at the optimal discharge pressure condition for the largest system COP. It could be observed that the inlet vapor quality of the two system were both less affected by the increasing superheat of air heat exchanger 2. However, the outlet vapor quality of system 2 was much smaller than that of system 1.

As for system 1, when the superheat degree of the air heat exchanger 2 was set as 1 °C, the flow vapor quality increased from 0.23 to 0.94 along the channel of battery cold-plate. The increment of the vapor quality was about 0.71, and this was the potential factor for the temperature non-uniformity of the battery. Besides, the higher vapor quality of 0.94 would result in the risk of thermal runaway propagation, especially caused by the flow inhomogeneous. This problem would be improved for the larger superheat degree of air heat exchanger 2, but the value of vapor quality and its increment were still at a higher level. The literal revealed a similar result that the vapor quality at the chiller exit easily reached to 0.9 or even superheated, and the battery temperature would be increased [39]. During the practical engineering, this phenomenon was deteriorated by the control stabilities and flow distributions.

With respect to system 2, the value of vapor quality at outlet of battery chiller was less affected by the superheat degree of air heat exchanger 2. Meanwhile, the vapor quality increment was only 0.17, which was much smaller than that of system 1. As the literal revealed that the battery maximum temperature was dramatically dropped with the decreasing vapor fraction in the chiller channel [25]. Thus, system 2 would have a better cooling performance with the smaller temperature difference. This provided huge margin for the actual control instabilities in two-phase refrigerant battery cooling, and it enhanced the thermal safety.

Thus, the proposed novel system had a smaller increase of the vapor quality along the channel of battery cold-plate, and it was easy to control, avoiding the thermal run away problem during the actual engineering.

When the battery heat load dropped from 0.5 kW to 0.2 kW, the battery chiller outlet vapor quality of the two system both declined. Nevertheless, the traditional system 1 still had a varied vapor quality inside the battery cooling channel. In the case, as the superheat degree of the air heat exchanger increased from 1 to 5, the vapor quality of traditional system 1 turned from 0.61 to 0.86, but the one of system 2 nearly remained the constant value of 0.3. As observed in Figs. 4 and 5, the increment of the vapor quality inside the battery cooling channel

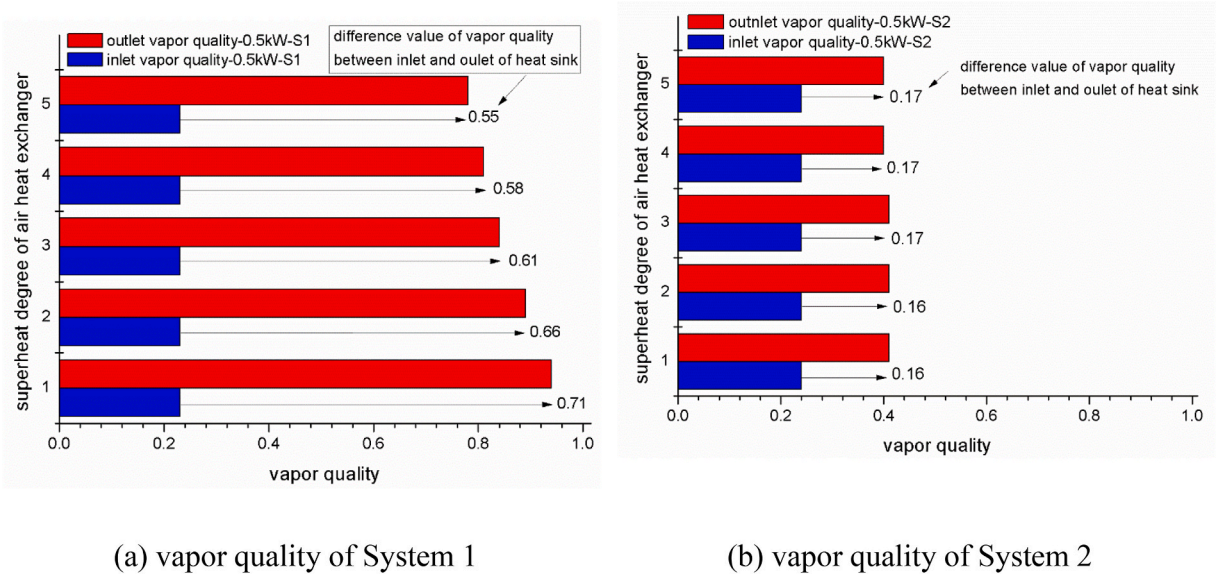

Fig. 4. Inlet and outlet vapor quality of the battery cold-plate at 0.5 kW power with the increasing superheat degree of air heat exchanger.

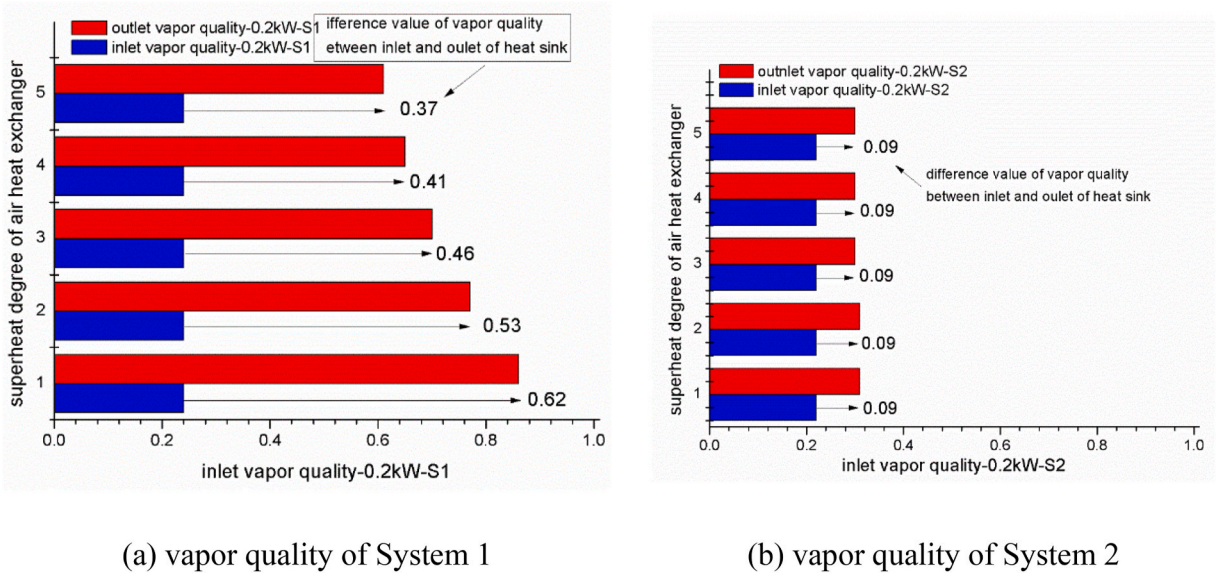

Fig. 5. Inlet and outlet vapor quality of the battery cold-plate at 0.2 kW power with the increasing superheat degree of air heat exchanger.

were affected by the battery heat load. The novel system 2 always provided a more stable boiling process, with a larger margin for the local superheating caused by the control and flow instabilities.

4.3. Performance comparison of the novel system

Besides the stabilities of the vapor quality in the battery cold-plate channel, the comprehensive energy efficiency was also the important parameters for the thermal management systems. Fig. 6 compares the energy efficiency of the novel system with the conventional ones. It could be obviously observed that the system COP of the novel system was always larger than that of the conventional one under the different discharge pressure operation condition. At the optimum state of the two system, the COP of the novel system was 0.29 (13.5%) bigger than the one of the conventional systems. Although the system COP both increased with discharge pressure and slightly decreased after the peaking value, the novel system in the presented study reached the maximum COP at a lower rejection pressure. This could be deeply reflected by the p-h diagram in Fig. 7. The novel system 2 worked at a higher evaporative and suction pressure, resulting in the larger COP.

As for the superheated temperature of the HX2, it slightly affected the COP of the conventional system configuration, but act insignificantly on the system performance of the novel systems. This indicated that the novel system was less affected by the control instabilities that caused the fluctuation of the superheated degree.

In the HVAC, there were two heat exchangers used as evaporator for the cooling purpose, and the cooling capacities of the two air heat exchangers was the main factor that affected the exchanger design. Fig. 6 illustrates the cooling capacity ratio of the two air heat exchangers, and the ratio was defined as follows.

$$Raito = Q_{HX2}/Q_{HX1}$$

As seen in Fig. 8, the cooling capacity ratio of the conventional system (S1) dropped dramatically with the increasing discharge pressure initially and then slowly decreased. However, the discharge pressure nearly had little influence on the ratio of the novel system (S2). In

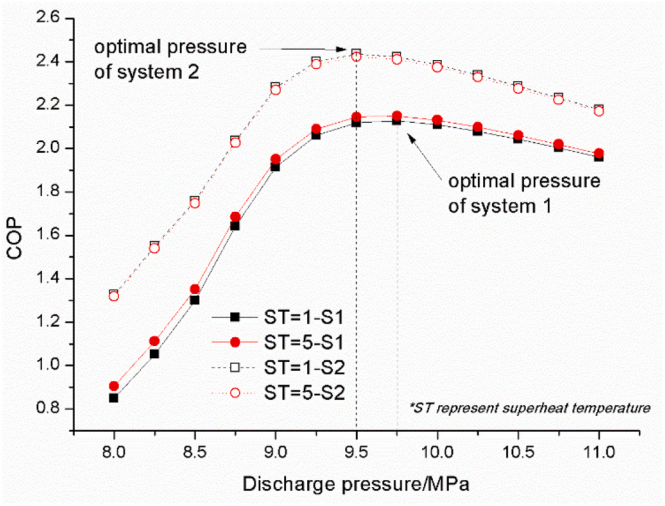

Fig. 6. Energy coefficient of the two systems.

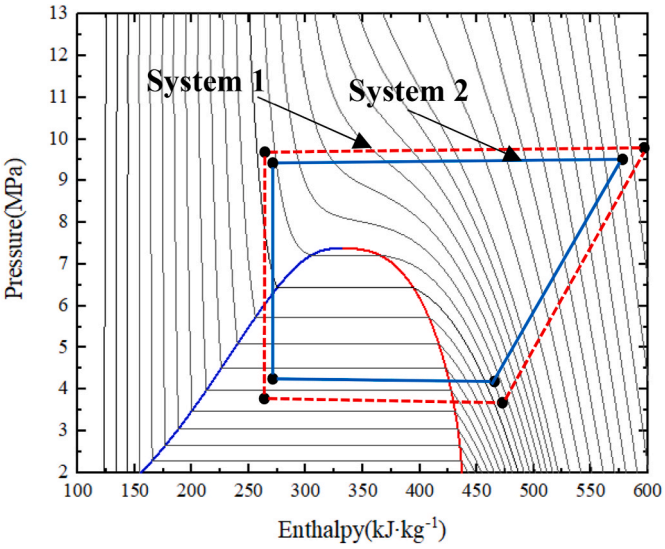

Fig. 7. The p-h diagram of the two systems.

other words, the distributions of the cooling capacity for the two heat exchangers varied heavily in the conventional system (S1) at different discharge pressure, but for the novel system configuration the discharge pressure would not influence the cooling capacity in each air heat exchanger.

Additionally, the ratio in Fig. 8 of the novel system 2 was always around 1.0, and it represented that it has a similar cooling capacity in each air heat exchanger.

4.4. Flow rate distributions

For the integrated thermal management systems in electric vehicles, the comprehensive coefficient of system performance and battery cooling results were the two main important parameters. The performance in the two-phase evaporative cooling was mostly affected by the vapor quality and the mass velocity, besides the channel structure.

Fig. 9 and Fig. 10 give the flow rate distributions of the two branches with and without the battery. For system 1, the flow rate distributions were strongly influenced by the system configuration and control method. A smaller flow velocity would cause the potential poorer cooling performance, with the higher risk of thermal runaway. As seen

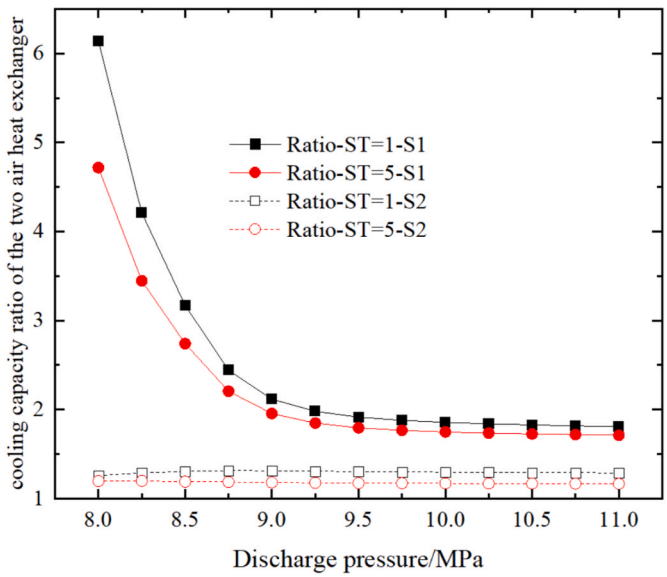

Fig. 8. Heating capacity ratio of the two-heat exchanger in HVAC.

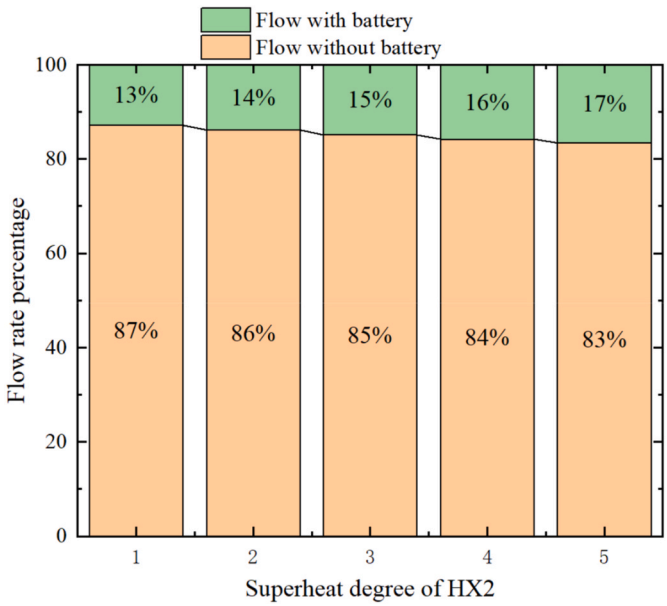

Fig. 9. Flow rate distributions in the two branch with and without battery cold-plate of conventional system 1.

in Fig. 9, most part of the refrigerant flowed through the heat exchanger that was without the battery. In other words, the mass velocity flowed into the battery cold-plate was much smaller. With the increase of the superheat temperature of HX2, the flow rate percentage in the battery cold-plate slightly rose to 17%.

However, it could be obviously observed in Fig. 10 that it has an apparent different flow rate distributions of the two branches in system 2, and the flow velocity was almost equally divided. When the two system both worked at the same operation condition, the battery cold-plate in the presented novel system 2 had nearly 3.5–4.5 times higher flow velocity than that of system 1. Thus, the novel system 2 had a better potential cooling permeance and lower risk of thermal runaway problem during the practical engineering.

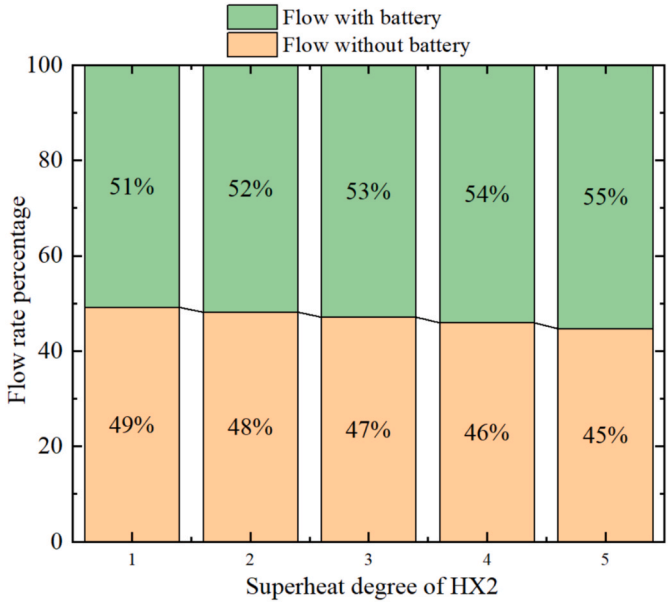

Fig. 10. Flow rate distributions in the two branch with and without battery cold-plate of novel system 2.

5. Conclusions and prospect

To deal with the potential thermal runaway problem due to the control instabilities of two-phase evaporative cooling, a novel integrated thermal management system based on transcritical CO2 cycles was proposed and theoretically investigated in the presented paper. As the literature revealed that the vapor quality in the two-phase colling cold plate heavily affected the cooling results, the vapor quality at the inlet and outlet in the cold plate of the two systems were studied and analyzed.

Results showed that the novel presented system had a smaller vapor quality at the outlet of the battery chiller, and its increment along the channel was both minor. Under the condition of 0.5 kW battery power, the flow vapor quality along the channel increased from 0.23 to 0.94 of the conventional systems, while it only ranged from 0.23 to 0.4 in the proposed system. Additionally, the presented systems had 13.5%higher COP at the ambient temperature of 35 °C. For the comprehensive coefficient of the system performance, the value of the novel system was also larger than that of the conventional one. Meanwhile, it reached the optimum performance at a smaller discharge pressure. The cooling capacity ratio of the two-air heat changer in the cabin was less affected by the discharge pressure, while it varied heavily in the conventional systems. The flow rate of the two branches in presented system was almost equally divided, while it only had a small part of refrigerant that flowed through the battery cold plate in the convention one.

As a conclusion, the proposed system configuration in the paper had a smaller vapor quality increment, higher system performance, more stable cooling capacity distributions and higher mass velocity in the clod plates. It could ensure the two-phase state and avoid the superheating at the outlet of the heat sink, which would have a less risk of thermal runaway problem. The results of the paper provided a more stable and better performance in the two-phase cooling systems with an easy superheated control.

Author contribution

Feng Cao provided guidance and supervision, Xiang Yin implemented the main research, discussed the results, and wrote the paper, Jianmin Fang provide help for formal analysis; Anci Wang curated the data; Yulong Song provide help for the revision of the paper. Xiaolin Wang revised the manuscript. All authors read and approved the final manuscript.

Declaration of competing interest

The authors declare that they have no known competing financial interests or personal relationships that could have appeared to influence the work reported in this paper.

Data availability

Data will be made available on request.

Acknowledgements

We are grateful to the National Natural Science Foundation of China [grant number 52006162, 51976153], and the Foundation for Innovative Research Groups of the National Natural Science Foundation of China [No. 51721004] for funding this research. The authors also thank the editors and reviewers for their comments and contribution to this manuscript.

References

[1] Pks A, Fl B. Diversity in transportation: why a mix of propulsion technologies is the way forward for the future fleet [J]. Results Eng., 4: 100060.
[2] A. García, J. Monsalve-Serrano, Analysis of a series hybrid vehicle concept that combines low temperature combustion and biofuels as power source, Results Eng. 1 (2019), 100001.
[3] Y. Guo, T. Wang, X. Liu, M. Zhang, X. Peng, Mathematical modelling and design of the ionic liquid compressor for the hydrogen refuelling station, Int. J. Energy Res. 46 (13) (2022) 19123–19137.
[4] X. Lai, M. Dai, R. Rameezdeen, Energy saving based lighting system optimization and smart control solutions for rail transportation: evidence from China, Results Eng. 5 (2020), 100096.
[5] V. Mali, R. Saxena, K. Kumar, A. Kalam, B. Tripathi, Review on battery thermal management systems for energy-efficient electric vehicles, Renew. Sustain. Energy Rev. 151 (2021), 111611.
[6] T. Wang, K.J. Tseng, J. Zhao, Development of efficient air-cooling strategies for lithium-ion battery module based on empirical heat source model, Appl. Therm. Eng. 90 (2015) 521–529.
[7] G. Zhang, F. Qin, H. Zou, C. Tian, Experimental study on a dual- parallel-evaporator heat pump system for thermal management of electric vehicles, Energy Proc. 105 (2017) 2390–2395.
[8] K. Liang, M. Wang, C. Gao, B. Dong, C. Feng, X. Zhou, J. Liu, Advances and challenges of integrated thermal management technologies for pure electric vehicles, Sustain. Energy Technol. Assessments 46 (2021), 101319.
[9] Z. Ling, F. Wang, X. Fang, X. Gao, Z. Zhang, A hybrid thermal management system for lithium ion batteries combining phase change materials with forced-air cooling - ScienceDirect, Appl. Energy 148 (2015) 403–409.
[10] J. Liang, Y. Gan, Y. Li, M. Tan, J. Wang, Thermal and electrochemical performance of a serially connected battery module using a heat pipe-based thermal management system under different coolant temperatures, Energy 189 (PT.1) (2019) 116233.1–116233.16.
[11] Y. Lyu, A.R.M. Siddique, S.A. Gadsden, S. Mahmud, Experimental investigation of thermoelectric cooling for a new battery pack design in a copper holder, Results Eng. 10 (2021), 100214.
[12] R.D. Widyantara, M.A. Naufal, P.L. Sambegoro, I.P. Nurprasetio, F. Triawan, D. W. Djamari, A.B.D. Nandiyanto, B.A. Budiman, M. Aziz, Low-cost air-cooling system optimization on battery pack of electric vehicle, Energies 14 (23) (2021) 7954.
[13] A.K. Thakur, R. Prabakaran, M.R. Elkadeem, S.W. Sharshir, M. Arıcı, C. Wang, W. Zhao, J.-Y. Hwang, R. Saidur, A state of art review and future viewpoint on advance cooling techniques for Lithium–ion battery system of electric vehicles, J. Energy Storage 32 (2020), 101771.
[14] Y. Li, K. Li, Y. Xie, B. Liu, J. Liu, J. Zheng, W. Li, Optimization of charging strategy for lithium-ion battery packs based on complete battery pack model, J. Energy Storage 37 (2021), 102466.
[15] T. Deng, G. Zhang, Y. Ran, P. Liu, Thermal performance of lithium ion battery pack by using cold plate, Appl. Therm. Eng. 160 (2019), 114088.
[16] D. Karimi, H. Behi, J. Van Mierlo, M. Berecibar, Experimental and numerical analysis of holistic active and passive thermal management systems for electric vehicles: fast charge and discharge applications, Results Eng. 15 (2022), 100486.
[17] M. Al-Zareer, I. Dincer, M.A. Rosen, A novel approach for performance improvement of liquid to vapor based battery cooling systems, Energy Convers. Manag. 187 (2019) 191–204.
[18] M. Shen, Q. Gao, Structure design and effect analysis on refrigerant cooling enhancement of battery thermal management system for electric vehicles, J. Energy Storage 32 (2020), 101940.

[19] R.W. van Gils, D. Danilov, P.H.L. Notten, M.F.M. Speetjens, H. Nijmeijer, Battery thermal management by boiling heat-transfer, Energy Convers. Manag. 79 (2014) 9–17.
[20] Z. An, L. Jia, X. Li, Y. Ding, Experimental investigation on lithium-ion battery thermal management based on flow boiling in mini-channel, Appl. Therm. Eng. 117 (2017) 534–543.
[21] M. Al-Zareer, I. Dincer, M.A. Rosen, Novel thermal management system using boiling cooling for high-powered lithium-ion battery packs for hybrid electric vehicles, J. Power Sources 363 (2017) 291–303.
[22] M. Al-Zareer, I. Dincer, M.A. Rosen, Heat and mass transfer modeling and assessment of a new battery cooling system, Int. J. Heat Mass Tran. 126 (2018) 765–778.
[23] V. Dhir, Boiling heat transfer, Annu. Rev. Fluid Mech. 30 (1) (1998) 365–401.
[24] D. Huang, H. Zhang, X. Wang, X. Huang, H. Dai, Experimental investigations on the performance of mini-channel evaporator refrigeration system for thermal management of power batteries, Int. J. Refrig. 130 (2021) 117–127.
[25] Y.-F. Wang, J.-T. Wu, Thermal performance predictions for an HFE-7000 direct flow boiling cooled battery thermal management system for electric vehicles, Energy Convers. Manag. 207 (2020), 112569.
[26] R.J. da Silva Lima, J.M. Quibén, J.R. Thome, Flow boiling in horizontal smooth tubes: new heat transfer results for R-134a at three saturation temperatures, Appl. Therm. Eng. 29 (7) (2009) 1289–1298.
[27] Y. Fang, F. Ye, Y. Zhu, K. Li, J. Shen, L. Su, Experimental investigation on system performances and transient response of a pumped two-phase battery cooling system using R1233zd, Energy Rep. 6 (2020) 238–247.
[28] J. Ma, Y. Sun, S. Zhang, J. Li, S. Li, Experimental study on the performance of vehicle integrated thermal management system for pure electric vehicles, Energy Convers. Manag. 253 (2022), 115183.
[29] Z. Tian, W. Gan, X. Zhang, B. Gu, L. Yang, Investigation on an integrated thermal management system with battery cooling and motor waste heat recovery for electric vehicle, Appl. Therm. Eng. 136 (2018) 16–27.
[30] D. Wang, B. Yu, J. Hu, L. Chen, J. Shi, J. Chen, Heating performance characteristics of CO2 heat pump system for electrical vehicle in a cold climate, Int. J. Refrig. 85 (2018) 27–41.
[31] D. Junqi, W. Yibiao, J. Shiwei, Z. Xianhui, H. Linjie, Experimental study of R744 heat pump system for electric vehicle application, Appl. Therm. Eng. 183 (2021), 116191.
[32] H. Zou, T. Yang, M. Tang, C. Tian, D. Butrymowicz, Ejector optimization and performance analysis of electric vehicle CO2 heat pump with dual ejectors, Energy 239 (2022), 122452.
[33] Y. Wang, D. Wang, B. Yu, J. Shi, J. Chen, Experimental and numerical investigation of a CO2 heat pump system for electrical vehicle with series gas cooler configuration, Int. J. Refrig. 100 (2019) 156–166.
[34] Y. Chen, H. Zou, J. Dong, J. Wu, H. Xu, C. Tian, Experimental investigation on the heating performance of a CO2 heat pump system with intermediate cooling for electric vehicles, Appl. Therm. Eng. 182 (2021), 116039.
[35] X. Yin, A. Wang, J. Fang, F. Cao, X. Wang, Coupled effect of operation conditions and refrigerant charge on the performance of a transcritical CO2 automotive air conditioning system, Int. J. Refrig. 123 (2021) 72–80.
[36] J. Fang, X. Yin, A. Wang, X. Sun, Y. Liu, F. Cao, Cooling performance enhancement for the automobile transcritical CO2 air conditioning system with various internal heat exchanger effectiveness, Appl. Therm. Eng. 196 (2021), 117274.
[37] F.W. Dittus, L. Boelter, Heat transfer in automobile radiators of the tubular type, Int. Commun. Heat Mass Tran. 12 (1) (1985) 3–22.
[38] S. Sisavath, X. Jing, C.C. Pain, R.W. Zimmerman, Creeping flow through an axisymmetric sudden contraction or expansion, J. Fluid Eng. 124 (1) (2002) 273–278.
[39] S.H. Hong, D.S. Jang, S. Park, S. Yun, Y. Kim, Thermal performance of direct two-phase refrigerant cooling for lithium-ion batteries in electric vehicles, Appl. Therm. Eng. 173 (2020), 115213.